# Origin of siderite mineralization in western Guizhou, SW China: Constrains from REEs, C, O, Sr and S isotopes

Xiao-Wen Huang [a], Liang Qi [b,*], Yu-Miao Meng [a], Da Chen [c], Hu-Dong Ling [c]

[a] State Key Laboratory of Ore Deposit Geochemistry, Institute of Geochemistry, Chinese Academy of Sciences, Guiyang 550002, China
[b] State Key Laboratory of Continental Dynamics, Department of Geology, Northwest University, Xi'an 710069, China
[c] Institute of Geological and Mineral Exploration, Non-ferrous Metals and Nuclear Industry Geological Exploration Bureau of Guizhou, Guiyang 550005, China

## ARTICLE INFO

## ABSTRACT

Numerous siderite deposits in western Guizhou of SW China are mainly hosted in the Middle Devonian dolostones. The larger Caiyuanzi (CYZ) and Xiongxiongjia (XXJ) deposits have an ore reserve in excess of 300 Mt with an average ore grade of ~35% total iron. There are banded and massive siderite ores and sulfide–siderite ores. The major ore mineral is magnesian siderite and gangue minerals are ankerite, dolomite, kaolinite, quartz and carbon. There are also metallic minerals including pyrite, chalcopyrite, and minor galena, tetrahedrite and enargite.

Rare earth elements (REEs) and carbon, oxygen, and strontium isotope data indicate a marine origin of the host dolostones and a hydrothermal metasomatic origin of the siderite mineralization. The variations of REEs and carbon and oxygen isotopic compositions of siderite from the CYZ and XXJ deposits reflect the variable mineralization processes and different fluid/rock ratios. The LREE depletion of siderite from the CYZ deposit could be due to crystallographic control, whereas the LREE depletion along with MREE enrichment and positive Eu anomalies of siderite from the XXJ deposit was possibly controlled by both crystallography and fluid composition. Siderite and calcite have $\delta^{13}C_{PDB}$ and $\delta^{18}O_{SMOW}$ values ranging from $-8$ to $-4.01‰$ and from 13.42 to 20.07‰, respectively. The variations in C and O isotopic compositions of siderite and calcite may reflect metasomatic replacement of marine carbonates by hydrothermal fluids at different fluid/rock ratios. Dolostones have $(^{87}Sr/^{86}Sr)_{initial}$ values of 0.70844–0.70920, whereas siderite and calcite have values ranging from 0.71396 to 0.71708. Negative correlations of initial Sr isotope ratios versus carbon and oxygen isotopes of the host dolostones, siderite and calcite indicated that carbonate minerals were metasomatic products of marine carbonates by hydrothermal fluids leaching from the Proterozoic basement rocks. Iron was possibly derived from the basement leaching rather than from the continental weathering. The $\delta^{34}S_{CDT}$ values ($-19.9$ to $13.6‰$) of sulfides associated with siderite indicated that the sulfur was probably derived from the marine sulfates through either bacterial sulfate reduction or organic mediated thermochemical reduction.

© 2014 Elsevier B.V. All rights reserved.

## 1. Introduction

Numerous Fe deposits are distributed in western Guizhou of China, which include the Caiyuanzi, Tiekuangshan, Xiongxiongjia, Guanyinshan and Guanziyao deposits from north to south (Fig. 1). The ore reserves of these deposits account for 72% total ore reserve of Fe deposits in Guizhou province (Li et al., 1996). The Fe orebodies occur as stratabound, stratoid, vein, and lenticular bodies and are mainly hosted in the Devonian carbonates and locally in the Lower Carboniferous carbonates. The ore genesis of these Fe deposits has been a matter of debate. These deposits were considered to be typical sedimentary deposits, hydrothermal or hydrothermal-reworked sedimentary deposits (Liao et al., 1984 and references therein). Continental weathering was considered to be the principal source of the iron.

In this study, we describe the geology of the larger Caiyuanzi and Xiongxiongjia deposits in West Guizhou with emphasis on the siderite mineralization. We obtain REE concentrations, carbon, oxygen and strontium isotopes of the host dolostones, siderite and calcite, and sulfur isotopes of sulfides. The new dataset is used to constrain the origin of the two deposits. An integrated model for siderite mineralization in western Guizhou is also proposed.

## 2. Geological setting

### 2.1. Regional geology

West Guizhou is situated at the western part of the Yangtze Block. The Yangtze Block is separated from the North China Craton by the Triassic Qinling–Dabie–Sulu orogenic belt to the north and bounded by the Tibetan Plateau to the northwest (Fig. 1a). To the southeast, the Yangtze Block is separated from the Cathaysia Block by a Neoproterozoic suture zone most likely formed at ~830 Ma (e.g. Zhao et al., 2011; Zhou et al., 2009). The Yangtze Block consists of a late Archean basement overlain by a Neoproterozoic to Cenozoic cover. The crystalline basement is represented by ~2.9 to 3.3 Ga tonalitic–trondhjemitic–granodioritic (TTG) rocks in the northern part of the Yangtze Block (e.g. Gao et al., 2011; Qiu et al., 2000). Paleo- to Mesoproterozoic strata exposed mainly in the western Yangtze Block are represented by the ~1.7 Ga Dongchuan and ~1.0 Ga Huili Groups (e.g. Sun et al., 2009; Zhao, 2010), which are considered to represent the folded basement (e.g. Yan et al., 2003). The cover sequences consist mainly of Paleozoic and Lower Mesozoic strata of shallow marine origin (Yan et al., 2003; Zhou et al., 2002).

The strata in western Guizhou include Early Paleozoic, Devonian, Carboniferous, Permian, and Mesozoic–Cenozoic strata (Fig. 1b). The Early
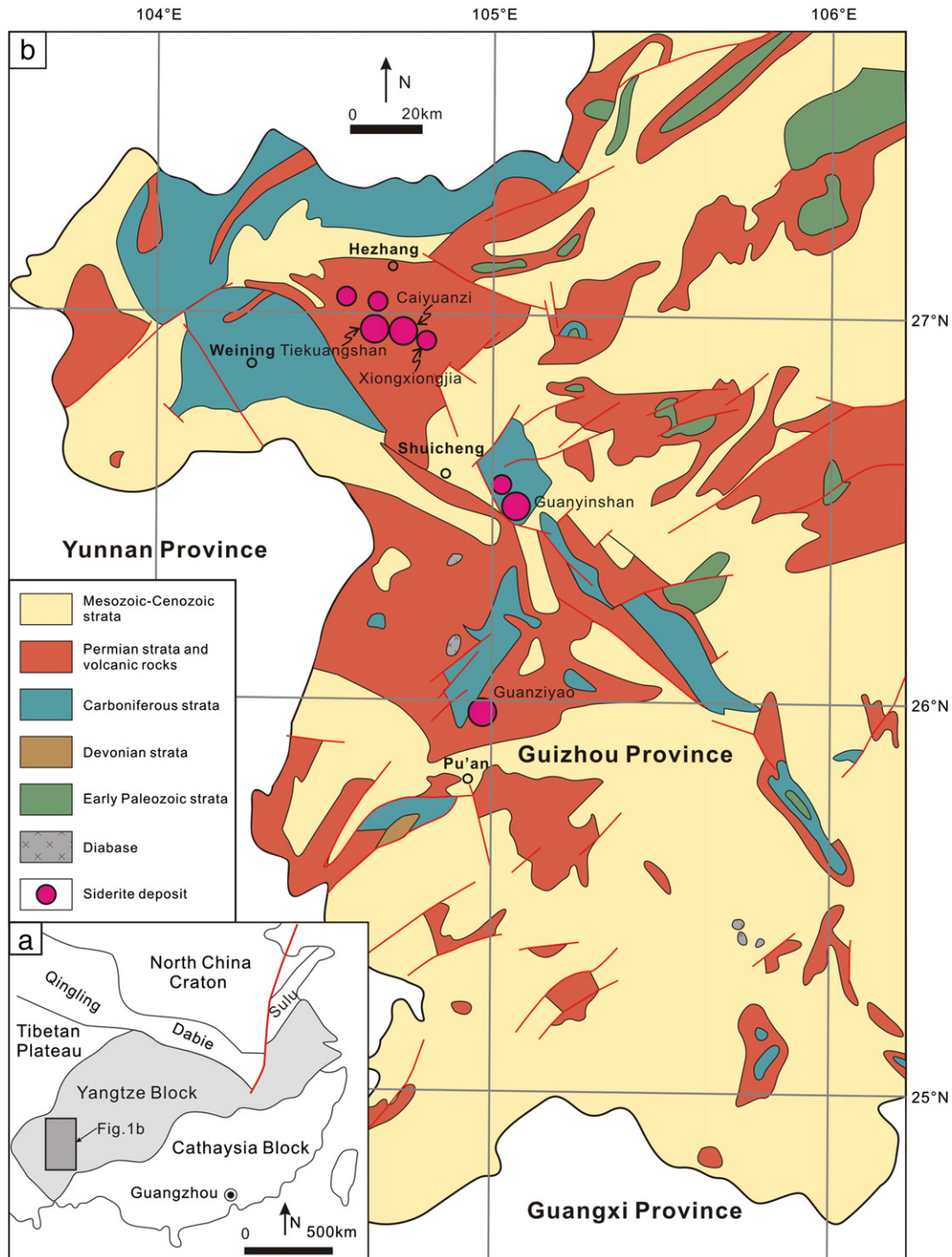


**Fig. 1.** (a) The location of West Guizhou in the Yangtze Block; (b) Geologic map showing the distribution of Fe deposits in the western Guizhou of SW China (modified from Liao et al., 1980). Because iron deposits are hosted in the Devonian strata that overlaid by Permian strata, these deposits are seemingly hosted in Permian strata as shown in figure (b).

Paleozoic strata are composed of argillaceous limestone, dolostone, and sandstone. The Carboniferous–Cenozoic strata are very similar in composition and consist of argillaceous/bioclastic limestone, argillaceous dolostone, sandstone, mudstone and minor carbonaceous shale and claystone. The Permian and Triassic strata locally contain thin layers of bitumen and coal. The Lower Devonian Danlin Group mainly consists of sandstone, whereas the Lower Devonian Shujiaping formation is composed of sandstone and argillaceous dolostone with minor dolomitic sandstone and limestone that host minor stratified siderite orebodies (Fig. 2). The Middle Devonian Longdongshui and Dushan formations are dominantly dolostone and limestone that host stratified, stratoid, or lenticular siderite orebodies, whereas the Middle Devonian Bangzhai formation is composed of sandy mudstone that hosts oolitic hematite and chamosite siderite orebodies (Fig. 2).

The volcanic rocks in western Guizhou are dominantly Permian flood basalts, which have $(^{87}Sr/^{86}Sr)_i$ values (calculated at 260 Ma) ranging from 0.704863 to 0.706602 (Qi and Zhou, 2008). Minor diabases intruded the Carboniferous to Triassic strata, which have ages ranging from 280 to 240 Ma and from 150 to 120 Ma (Liao et al., 1984). There is no contact metamorphism within the contact zone between diabases and wall rocks and no direct contacts between diabases and siderite orebodies.

### 2.2. Deposit geology

The Caiyuanzi and Xiongxiongjia Fe deposits were discovered by the Bureau of Geology and Mineral Exploration and Development of Guizhou Province in the 1970s (Li et al., 1996). The Caiyuanzi (CYZ) deposit has an ore reserve of ~120 Mt (million tons) with an average grade of ~36% total iron, whereas the Xiongxiongjia (XXJ) deposit was estimated to have an ore reserve of >160 Mt with an average grade of ~32% total iron (Li et al., 1996).

The CYZ deposit consists of more than 100 orebodies, with four main orebodies. Two types of mineralization at the CYZ deposit include hematite and siderite mineralization (Fig. 3a and b). Hematite mineralization is not referred to in this study. The siderite orebodies are hosted in the dolostone and argillaceous dolostone of the Middle Devonian Dushan and Longdongshui formations and the Lower Devonian Shujiaping formation (Fig. 3a and b). The mineralization zone is 5 km long and 200 to 1800 m wide along strike and down dip, respectively, consisting of >123 orebodies. More than 10 orebodies have individual ore reserves of more than 1 Mt. The main orebodies have a length of 460 to 1800 m, a width of 80 to 460 m, and an average thickness of 14.1 m (Li et al., 1996). The siderite ores have ore grades of 32.5–37.6% total iron (Li et al., 1996). The ores and dolostones have average organic carbon contents of 0.38% and 0.22%, respectively (Liao et al., 1984).

The XXJ deposit has not been mined and was explored by drillholes and trenching (Fig. 4a). Mineralization types also include hematite and siderite Fe mineralization (Fig. 4b). Siderite orebodies of the XXJ deposit are hosted in the carbonate rocks of the Middle Devonian Dushan and Longdongshui formations (Fig. 4b). The upper wall rocks are fine-grained dolostones, whereas the bottom wall rocks are fine-grained quartz sandstones. There are clear boundaries between orebodies and wall rocks, which are nearly paralleled to the strike of strata.

Ore types of the CYZ and XXJ deposits are similar. Siderite ores at the CYZ are banded and massive (Fig. 5a–c), which are composed of siderite, dolomite, calcite, quartz, organic materials, and sulfides such as chalcopyrite, pyrite, and galena (Fig. 6a–d). Siderite ores at

| Period | | Formation | Lithologic log | Thickness (m) | Petrographic description and mineralization |
|---|---|---|---|---|---|
| Devonian | Upper | Yaosuo | | >100 | The rocks are dolomitic limestones and minor dolostones. |
| | | Wang chengpo | | 150 | The rocks are dominantly dolomitic limestones with minor dolostones, which host stratoid siderite orebodies. |
| | Middle | Dushan | | 300-400 | Jiwozhai member: the rocks are dolostones and limestones, which host stratoid siderite orebodies such as (5) and (6) in Fig. 2a . |
| | | | | | Songjiaqiao member: the rocks are purple, sandy shales with minor dolostones and limestones. |
| | | | | | Jipao member: the rocks are dominantly dolostones, which host lenticular siderite orebodies such as (1) and (2) in Fig. 2a. |
| | | Bangzhai | | 50-150 | The rocks are grey dark, sandy mudstone, which host oolitic hematite and chamosite siderite. |
| | | Longdong shui | | 30-60 | The rocks are grey dark, sandy, and fine-grained dolostones, which host stratoid siderite orebodies (no. $II_1$ and $II_2$ in Fig. 2a). |
| | Lower | Shujiaping | | 20-30 | The upper part of this formation are sandstones and minor dolomitic sandstones, whereas the lower part are argillaceous dolostones with minor limestones. Minor stratified siderite orebodies occur in this formation. |
| | | Danlin | | 10-30 | Sandstone |

████ Fe mineralization

**Fig. 2.** Stratigraphic column of the Devonian showing Fe mineralization in the Caiyuanzi deposit (modified from Liao et al., 1980). Iron orebodies are mainly hosted in the Middle Devonian strata.
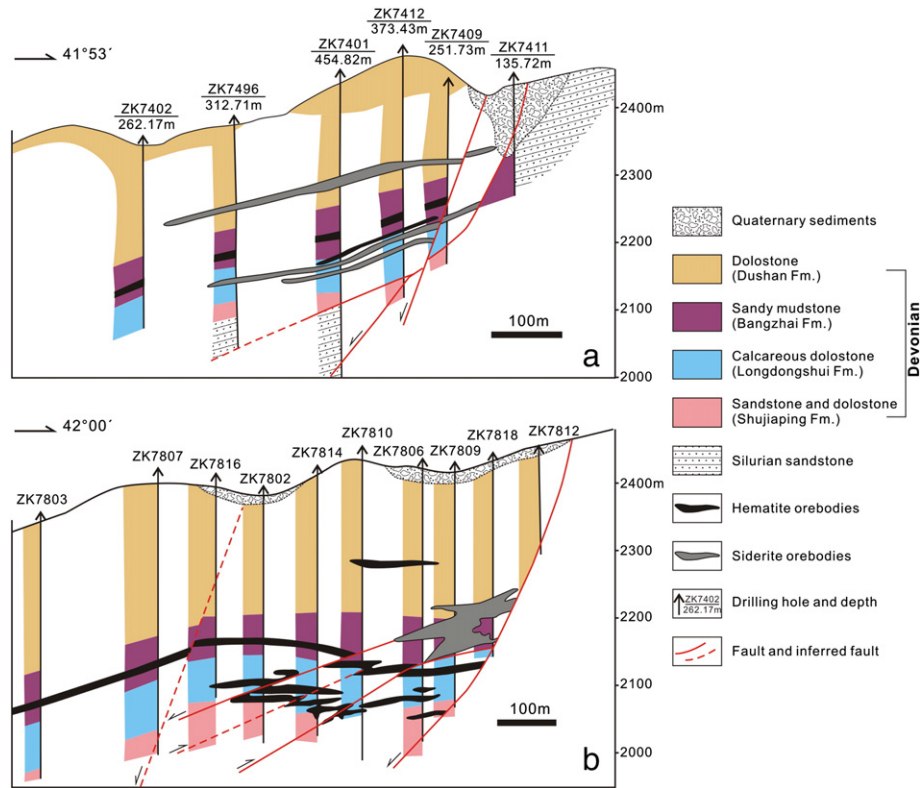
**Fig. 3.** Geologic section of prospecting lines of the Caiyuanzi deposit showing stratified and stratoid (a) and lenticular (b) siderite orebodies (modified from Liao et al., 1984). The stratified orebodies in figure a are crosscut by the later faults, indicating that these faults have destroyed the orebodies. The lenticular orebodies in figure b are obviously controlled by two parallel faults, indicating that the ore fluids may have transported along these faults and precipitated in a relatively open space.

the XXJ include banded, dark and light massive ores (Fig. 5d–f). Ores are composed of siderite, calcite, carbon, quartz and minor sulfides (Fig. 6e–h).

The paragenetic sequence of siderite mineralization in the western Guizhou of SW China is relatively simple (Fig. 7). Stage one is dominantly represented by sedimentation of the host dolostones, which has a mineral assemblage of dolomite, carbon, and pyrite (Fig. 6a). Following diagenesis is hydrothermal replacement of dolostones, forming ankerite and dark massive siderite ores (Fig. 6b and c). Organic carbon between siderite grains makes the ores dark. Stage three is the hydrothermal stage and the main mineralization stage. Light massive, banded and sulfide–siderite ores were formed at this stage, which have a mineral assemblage of siderite, pyrite, chalcopyrite, carbon, kaolinite, quartz, and minor tetrahedrite, enargite, and galena (Fig. 6d–h).

## 3. Samples and analytical techniques

Samples in this study were collected from the opencast CYZ deposit and the pitting and trenching of the XXJ deposit. Pure siderite, calcite, and chalcopyrite separates (0.5 to 1 g) were handpicked under a binocular microscope after crushing and sieving. The whole rock samples were trimmed to remove altered surfaces and were cleaned by distilled water and dried at 50 °C for 12 h. The whole rock samples were crushed and powdered by tungsten carbide ring grinder mill, whereas the mineral separates were powdered by agate mortar.

REEs, C, O and Sr isotopes were determined at the Institute of Geochemistry, Chinese Academy of Sciences (IGCAS). REEs were analyzed with a PE Elan DRC-e ICP-MS following the procedures described by Qi and Grégoire (2000). About 50 mg sample powder were digested with HF and $HNO_3$ in a PTFE-lined stainless steel bombs at 185 °C for 24 h, evaporated to dryness, and re-dissolved by 6 ml of 40% v/v $HNO_3$ at 140 °C for 3 h. The final solution for ICP-MS analyses was made up to 8 ml by diluting 0.4 ml sample solution using the deionized water.

Rhodium was used as an internal standard to correct for matrix effects and instrument drift. Precisions were typically better than 5% RSD.

Carbon and oxygen isotopic compositions were determined using a GasBench II device in the continuous flow mode coupled with a MAT 253 Isotope Ratio Mass Spectrometer (IRMS) following the equilibration method (Rangarajan and Ghosh, 2011). The carbon dioxide gas was extracted by reaction with 15 drops of pure phosphoric acid in a sealed quartz tube at 80 °C for 1 h and carried to mass spectrometer by helium gas. Carbon and oxygen isotope ratios afforded by IRMS are expressed as δ-notation in per mil (‰) relative to Vienna–Pee Dee belemnite (V–PDB). The oxygen isotope ratios are usually reported to be relative to Vienna–Standard Mean Ocean Water (V–SMOW) standard according to the formula $\delta^{18}O_{SMOW} = 1.03091 \times \delta^{18}O_{PDB} + 30.91$ (Coplen et al., 1983). Repeated analyses of Chinese carbonate standards GBW04416 (marble) and GBW04417 (calcite) yielded respective $\delta^{13}C_{PDB}$ values of 1.60 ± 0.04‰ and −6.14 ± 0.04‰ (1σ, n = 10) and respective $\delta^{18}O_{PDB}$ values of −11.56 ± 0.06‰ and −24.07 ± 0.06‰ (1σ, n = 10), in good agreement with the certified $\delta^{13}C_{PDB}$ values of 1.16 ± 0.03‰ and −6.06 ± 0.06‰ and $\delta^{18}O_{PDB}$ values of −11.59 ± 0.11‰ and −24.12 ± 0.19‰ (Zheng and Chen, 2000). The measured $\delta^{13}C_{PDB}$ (1.99 ± 0.04‰; 1σ, n = 10) and $\delta^{18}O_{PDB}$ (−2.15 ± 0.04‰; 1σ, n = 10) values of international standard NBS-19 (marble) are also consistent with the certified values of 1.95‰ and −2.2‰, respectively (Coplen, 1994).

Rubidium, Sr, Sm and Nd concentrations of carbonate minerals are determined by a PE Elan DRC-e ICP-MS using the same method as the REE determination. Due to low Nd contents for most siderite samples, Nd isotopes were not measured. Sample powders were dissolved in Teflon bombs with mixed acid of HF and $HNO_3$, followed by conventional cation-exchange techniques. Strontium isotopic ratios were determined by a Neptune MC-ICP-MS at the Chengdu University of Technology. Repeated analyses of NBS-987 Sr standard yielded an average $^{87}Sr/^{86}Sr$
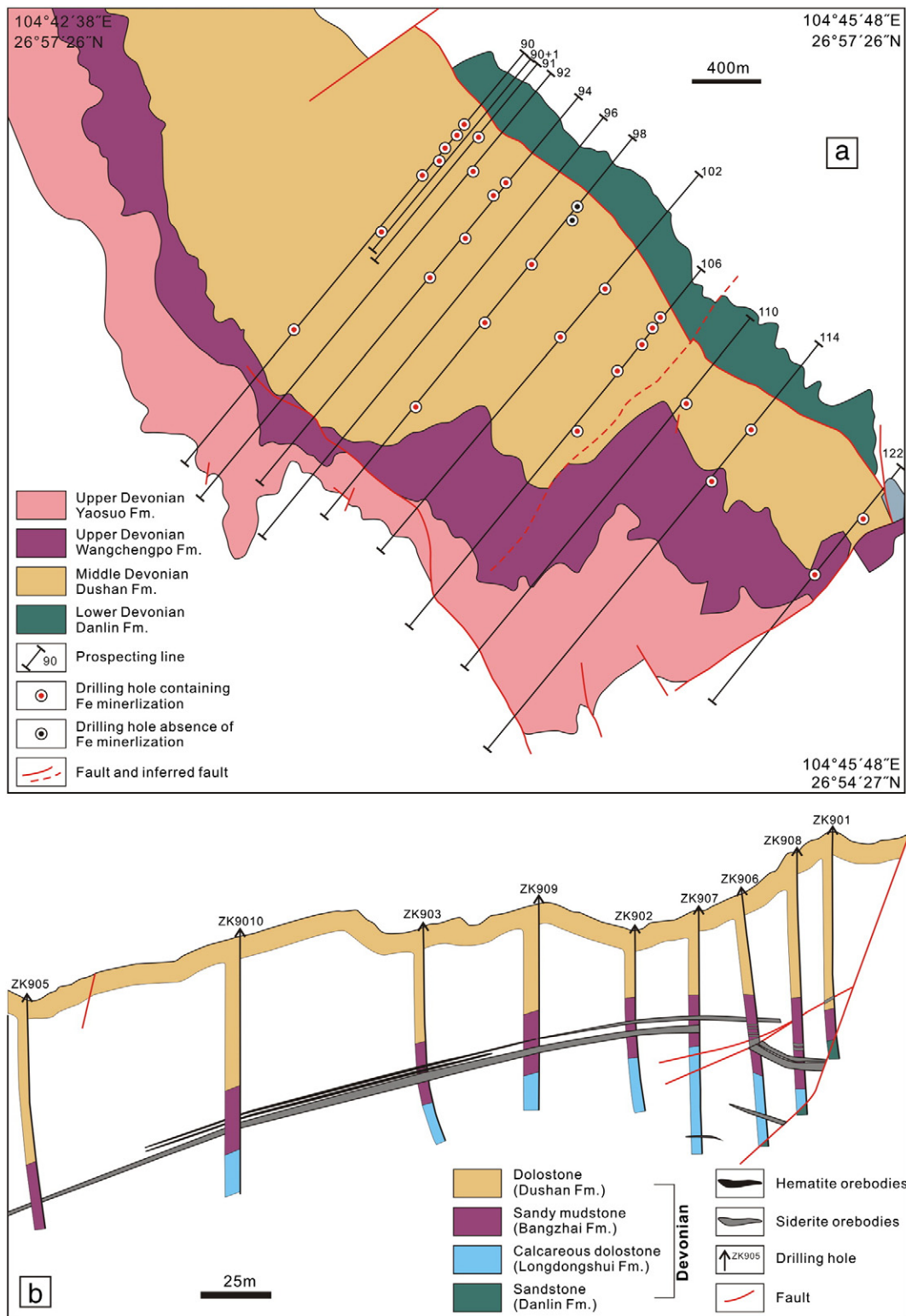
**Fig. 4.** (a) Simplified geological map of the Xiongxiongjia deposit showing the ore-hosting Devonian strata; (b) Geologic section of prospecting line 90 in figure a showing the distribution of Fe orebodies (modified from unpublished maps of Non-ferrous Metals and Nuclear Industry Geological Exploration Bureau of Guizhou).

value of 0.710341 ± 0.000029 (2σ, n = 25), in agreement with the certified value of 0.71034 ± 0.00026 (370 ppm) (NIST, certificate issue 1/5/2000).

Sulfur isotopes were analyzed using a EuroVector EA3000 element analyzer (EA) coupled to a GV IsoPrime IRMS (EA-IRMS). The method was similar to that described in Huang et al. (2013). The sulfur isotopic compositions are reported as δ-notation in per mil (‰) relative to Vienna–Canyon Diablo troilite standard (V–CDT). Replicate analyses of Chinese $Ag_2S$ standards, GBW04414 and GBW04415, yielded $\delta^{34}S$ values of −0.07 ± 0.09‰ (1σ, n = 27) and 22.33 ± 0.09‰ (1σ, n = 3), respectively, in good agreement with the certified values of −0.07 ± 0.13‰ and 22.15 ± 0.14‰ (1σ) (Ding et al., 2001).
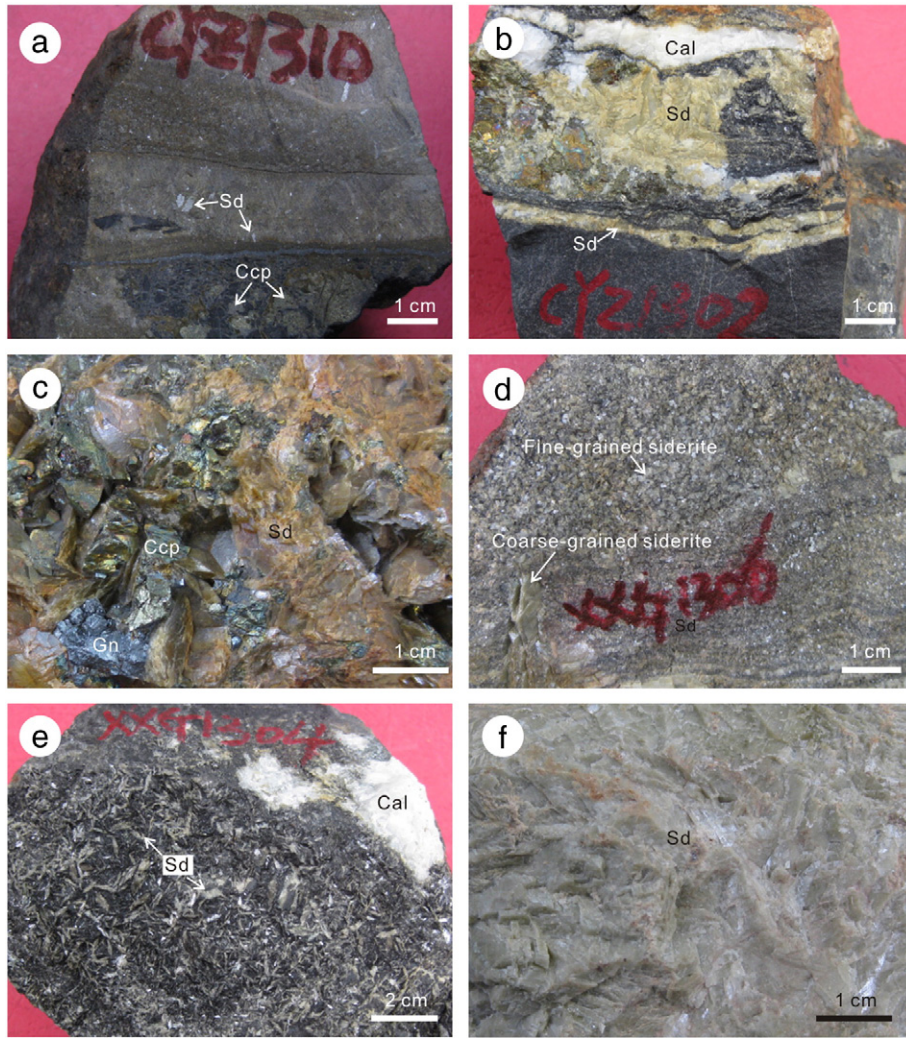
**Fig. 5.** Photos of different types of ores from the Caiyuanzi (CYZ) and Xiongxiongjia (XXJ) deposits. (a) Banded ore from the CYZ deposit composed of siderite, chalcopyrite; (b) Banded ore from the CYZ deposit consisting of siderite, chalcopyrite and calcite; (c) Sulfide-siderite ore from the CYZ deposit consisting of siderite, chalcopyrite and galena; (d) Banded ore from the XXJ deposit composed of fine-grained and coarse-grained siderite; (e) Massive ore from the XXJ composed of radial siderite and calcite; (f) Massive ore from the XXJ comprising coarse-grained siderite. Sd, siderite; Cal, calcite; Ccp, chalcopyrite; Gn, galena.

## 4. Analytical results

### 4.1. Rare earth elements

The REE contents and related ratios of the dolostones, siderite and calcite are presented in Table 1. REE patterns are shown in Fig. 8, normalized to post-Archean Australian shale (PAAS) (Nance and Taylor, 1976). Dolostones have 3.99 to 42.6 ppm total REE and show flat REE patterns (Fig. 8a) with no obvious fractionation among LREE and HREE except two outliers (($La/Yb)_N$ = 0.93 to 1.19) (Table 1). Dolostones show low to moderate MREE enrichment relative to HREE with ($Gd/Yb)_N$ ratios of 0.73 to 4.05. All dolostones show slightly positive Eu and Ce anomalies.

Siderite separates contain 0.84 to 5.74 ppm total REE, significantly lower than the dolostones (Table 1). Siderite separates from the CYZ deposit show left-inclined REE patterns (Fig. 8b) and have very low ($La/Yb)_N$ ratios (<0.1), ($La/Sm)_N$ ratios (0.02–0.51), ($Gd/Yb)_N$ ratios (0.09–0.68) and weakly positive or negative Eu anomalies ($\delta$Eu = 0.73–1.88), whereas those from the XXJ deposit are characterized by upward-convex REE patterns, with low ($La/Yb)_N$ ratios (0.03–0.35), low ($La/Sm)_N$ ratios (0.03–0.35), ($La/Yb)_N$ ratios (2.10–5.58), and positive Eu anomalies ($\delta$Eu = 1.34–2.74) and weakly positive or negative Ce anomalies ($\delta$Ce = 0.80–1.35) (Fig. 8b). Calcite separates have higher

total REE contents (9.72 to 13.5 ppm) than siderite separates, which also show upward-convex REE patterns with very low ($La/Yb)_N$ and ($La/Sm)_N$ ratios of ~0.01, high ($Gd/Yb)_N$ ratios of 2.99 to 4.44, and no Ce and Eu anomalies (Fig. 8c). Calcite has higher LREE and MREE contents but lower HREE contents than associated siderite (Fig. 8d). Fine-grained siderite has higher LREE contents than coarse-grained siderite from the same ore (Fig. 8d).

### 4.2. Carbon and oxygen isotopic compositions

Carbon and oxygen isotope data are listed in Table 2 and illustrated in Fig. 9. Dolostones have $\delta^{13}C_{PDB}$ and $\delta^{18}O_{SMOW}$ values ranging from −0.57 to 0.33‰ and from 25.99 to 26.35‰, respectively. Siderite samples from the CYZ and XXJ deposits have similar $\delta^{13}C_{PDB}$ and $\delta^{18}O_{SMOW}$ values ranging from −8 to −5.09‰ and from 13.42 to 20.07‰, respectively. Calcite samples from the two deposits also have similar $\delta^{13}C_{PDB}$ values of −4.01 and −4.86‰ and $\delta^{18}O_{SMOW}$ values of 18.91‰ and 18.25‰, respectively. Dolostones have heavier C and O isotopic compositions than siderite and calcite, whereas siderite and calcite have similar $\delta^{13}C_{PDB}$ and $\delta^{18}O_{SMOW}$ values (Fig. 9). There is a positive correlation ($R^2$ = 0.87) between $\delta^{13}C_{PDB}$ and $\delta^{18}O_{SMOW}$ values of siderite (Fig. 9).
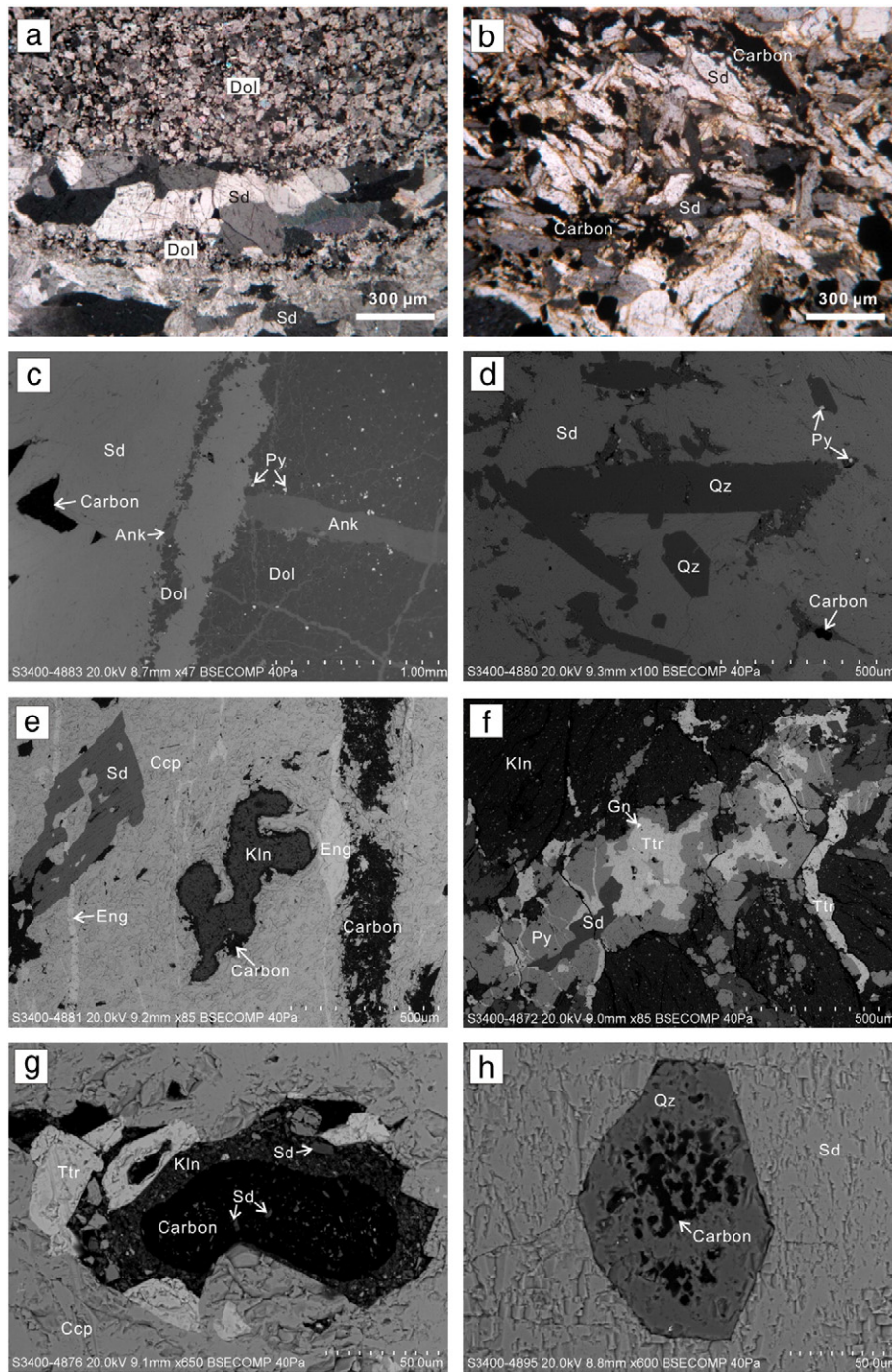
**Fig. 6.** Photomicrographs of ores from the CYZ and XXJ deposits. (a) Banded ore from the CYZ deposit composed of interbedded dolomite and siderite (under crossed polarized light). The sharp boundary between siderite and dolomite veins indicates that the siderite was formed by infilling the fractures of dolostone; (b) Dark massive ore from the XXJ deposit composed of euhedral siderite and carbon (under crossed polarized light); (c) Banded ore from the CYZ deposit composed of ankerite, dolostone, siderite, pyrite and carbon. Ankerite veins in the dolostone were cut by siderite veins, indicating that ankerite formed later than dolostone but earlier than siderite. Pyrite associated with dolomite indicates these pyrite grains were sedimentary in origin (BSE); (d) Banded ore from the CYZ deposit composed of euhedral quartz, siderite, pyrite, and carbon (BSE); (e) Sulfide-siderite ore from the CYZ deposit composed of chalcopyrite, enargite, siderite, kaolinite and carbon (BSE); (f) Dark massive ore from the CYZ deposit composed of pyrite, tetrahedrite, siderite, galena, and kaolinite. Pyrite was replaced by tetrahedrite and was crosscut by siderite indicating earlier formation of pyrite (BSE); (g) Dark massive ore from the CYZ deposit composed of chalcopyrite, carbon, kaolinite, tetrahedrite and minor siderite. Carbon was enclosed by kaolinite, indicating earlier formation of carbon (BSE); (h) Dark massive ore from the XXJ deposit consisting of siderite, quartz and carbon. Euhedral quartz and carbon enclosed in the siderite, indicating their earlier formation (BSE). Sd, siderite; Ank, ankerite; Dol, dolomite; Py, pyrite; Ccp, chalcopyrite; Gn, galena; Ttr, tetrahedrite; En, enargite; Kln, kaolinite; Qz, quartz.

### 4.3. Strontium isotopes

Dolostones have $(^{87}Sr/^{86}Sr)_i$ values ranging from 0.70844 to 0.70920, whereas siderite and calcite have more radiogenic $(^{87}Sr/^{86}Sr)_i$ values ranging from 0.71396 to 0.71709 (Table 3). The initial Sr isotope ratios of calcite lie within the range of these values in siderite. There are

no obvious correlations between $(^{87}Sr/^{86}Sr)_i$ and $^{87}Rb/^{86}Sr$ for the dolostones, siderite and calcite (Fig. 10a). There is a weak positive correlation between initial Sr isotope ratios and the reciprocal of Sr concentrations for dolostones and siderite (Fig. 10b). There are negative correlations between $(^{87}Sr/^{86}Sr)_i$ and $\delta^{13}C_{PDB}$ and between $(^{87}Sr/^{86}Sr)_i$ and $\delta^{18}O_{SMOW}$ for dolostones, siderite and calcite (Fig. 10c and d).

| Mineral \ Stage | Sedimentation | Hydrothermal metasomatic | Hydrothermal |
|---|---|---|---|
| Dolomite | ▬▬▬ | | |
| Chamosite | ▬▬▬ | | |
| Carbon | ▬ | ▬▬▬ | ▬▬ |
| Pyrite | ▬ | ▬▬▬ | ▬▬ |
| Siderite | | ▬▬▬ | ▬▬ |
| Kaolinite | | ▬▬▬ | |
| Quartz | ▬▬▬ | ▬▬ | |
| Ankerite | | | |
| Calcite | | | ▬▬ |
| Chalcopyrite | | | ▬▬▬ |
| Tetrahedrite | | | ▬ |
| Enargite | | | ▬ |
| Galena | | | ▬ |
| **Sample type** | Dolostone | Dark massive ore | Light massive ore / Banded ore / Sulfide-siderite ore |

**Fig. 7.** Paragenesis of siderite mineralization in western Guizhou of SW China.

### 4.4. Sulfur isotopic composition of sulfides

Sulfur isotope data of sulfides from the COC are presented in Table 4 and elaborated in Fig. 11. The $\delta^{34}S_{CDT}$ values of sulfides from the Caiyuanzi deposit cover a wide range between −19.9 and 13.6‰. Pyrite has larger variations of sulfur isotopic composition than chalcopyrite (Fig. 11a), with $\delta^{34}S_{CDT}$ values ranging from −19.9 to 11.6‰ for the former and from 2.4 to 13.6‰ for the latter, respectively. There are no obvious differences in sulfur isotopic composition of sulfides from the wall rocks and siderite ores (Fig. 11b).

## 5. Discussion

### 5.1. REE geochemistry

Normalized REE patterns of Ca, Mg, and Fe carbonates can be used to constrain the fluid and precursor mineral composition, or the transition of physicochemical conditions during mineralization (Bau and Möller, 1992). Most dolostones have similar total REE contents and flat REE patterns to marine sedimentary calcareous carbonates (Hu et al., 1988). However, the dolostones have slightly positive Eu and Ce anomalies ($\delta Eu = 1.10$–1.38 and $\delta Ce = 1.10$–1.18), which do not correspond to those of marine sedimentary carbonates with characteristic negative Ce anomaly (Elderfield and Greaves, 1982; Hu et al., 1988). This indicates that the host dolostones were locally modified by some hydrothermal fluids with significantly different REE contents during siderite formation.

The LREE depletion of siderite could be attributed to crystallographic control due to differences in ionic radii between $REE^{3+}$ and $Fe^{2+}$ (Morgan and Wandless, 1980). HREE are more easily incorporated in the siderite crystal lattice because of their smaller ionic radii than LREE and higher charge than $Fe^{2+}$ (Bau and Möller, 1992). The crystallographic control can only explain the REE patterns of siderite from the CYZ deposit but cannot be applicable to siderite from the XXJ deposit. The LREE depletion along with positive Eu anomalies and MREE enrichment of siderite from the XXJ deposit most likely reflect the fluid compositions (Castorina and Masi, 2008; Torres-Ruiz, 2006). These REE patterns are typical of high-temperature crustal- or oceanic-derived hydrothermal fluids that may have interacted with metasediments under acid conditions at low oxygen fugacities and high temperatures (>200–250 °C) (Hecht et al., 1999; Lüders et al., 1993; Michard, 1989), which results in the combination of LREE depletion (governed by chemical complexation) during hydrothermal remobilization of REE from deeper source rocks and HREE depletion as a result of scavenging by less soluble minerals during REE remobilization.

The similarity of REE patterns between siderite and calcite indicates their derivation from the same ore fluids. Calcite has higher LREE and MREE contents than associated siderite (Fig. 8d), which is consistent with the mineralogical control mechanism (Bau and Möller, 1992). The positive Eu anomalies in both calcite and siderite reveal that Eu was divalent during siderite and calcite formation, i.e., these carbonates precipitated in a low-T environment (<250 °C) from a hydrothermal solution which received its REE signature during fluid–rock interaction in a high-T environment. Moreover, the combination of positive Eu and negative Ce anomalies for some siderite separates (e.g. CYZ1308, XXJ1302, XXJ1303, and XXJ1306), which appears to be impossible in the same physicochemical environment, indicates that the siderite cannot represent original chemical sediments. The siderite was most likely to be the metasomatic product of a sedimentary carbonate precursor. Alternatively, fluid REE addition resulted in the disappearance of the negative Ce anomaly and the appearance of the pronounced positive Eu anomaly of the carbonate precursor. Therefore, REE composition indicates a hydrothermal metasomatic origin for siderite and calcite.

### 5.2. Carbon and oxygen sources

Carbon and oxygen isotopic composition of the dolostones are close to those ($0 \pm 3$‰ and ~28‰, respectively) of recent and Phanerozoic marine carbonates (Veizer and Hoefs, 1976), indicating that these dolostones are sedimentary in origin. The low $\delta^{13}C_{PDB}$ (−8.0 to −3.9‰) of siderite and calcite indicate that they are likely not marine diagenetic products and were derived from an external carbon sources because under reducing conditions in shallow burial methanogenesis would produce a heavy carbon isotopic composition (Baker et al., 1996; Irwin et al., 1977). Bacterial oxidation of organic carbon (methane, petroleum, or organic matter) would produce lower $\delta^{13}C_{PDB}$ values (Baker et al., 1996; Savard et al., 1998). Siderite ores and wall rocks from the CYZ deposit have mean organic carbon contents of 0.38 wt.% and 0.22 wt.%, respectively (Liao et al., 1984). Therefore, the carbon of carbonate minerals probably derived from some organic-rich materials. The similar organic origin of carbon has been proposed for siderite deposits from the Lombardy Valleys in Italy (Cortecci and Frizzo, 1993), for sideritized host rocks from the Walton Ba deposit in Canada (Savard et al., 1998), for late-stage carbonates related to talc mineralization at Göpfersgrün in Germany (Hecht et al., 1999), and for Marquesado siderite deposits in Spain (Torres-Ruiz, 2006). The $\delta^{18}O_{SMOW}$ values (13.4 to 21.5‰) of siderite and calcite are different from those (approximately from −24 to 8‰) of marine, freshwater, burial, and hydrothermal siderites, but similar to those (typically between ~14 and 20‰) of metasomatic siderite, calcite, and dolomite in marine carbonate rocks (e.g., Cortecci and Frizzo, 1993; Hecht et al., 1999; Palinkaš et al., 2009; Timofeyeva et al., 1976; Torres-Ruiz, 2006).

Fluid inclusions from the siderite and associated quartz veins have similar homogenization temperatures between 160 and 250 °C (Liao et al., 1984; Lin et al., 1986). Under such a temperature range, a fluid in equilibrium with siderite would have $\delta^{18}O_{SMOW}$ values of 0.2 to 10‰ using the appropriate fractionation factors ($10^3 \times \ln\alpha = 3.13 \times 10^6 \times T^{-2} - 3.50$; Carothers et al., 1988). These values are consistent with formation waters, $^{18}O$-shifted hydrothermal meteoric or magmatic waters, but exclude unmodified meteoric waters (Sheppard, 1986). Fluid inclusions in siderite were composed of Na–Cl brines with high salinities of 10.9–26.2 wt.% NaCl-equiv. (Liao et al., 1984), indicating formational or shield brines rather than dilute meteoric hydrothermal waters as mineralizing agents.

To examine the fluid evolution process for siderite and calcite formation, quantitative modeling calculation of C and O isotopes is performed using zero-dimensional water–rock interaction equations for open or closed systems (Zheng and Hoefs, 1993). In the modeling of siderite, we use initial carbonate rock with $\delta^{13}C_{PDB}$ and $\delta^{18}O_{SMOW}$ values of 2 and 28% (average composition of marine carbonate), one fluid with

**Table 1**
REE contents (ppm) of the dolostones, siderite and calcite from the Caiyuanzi and Xiongxiongjia deposits in western Guizhou.
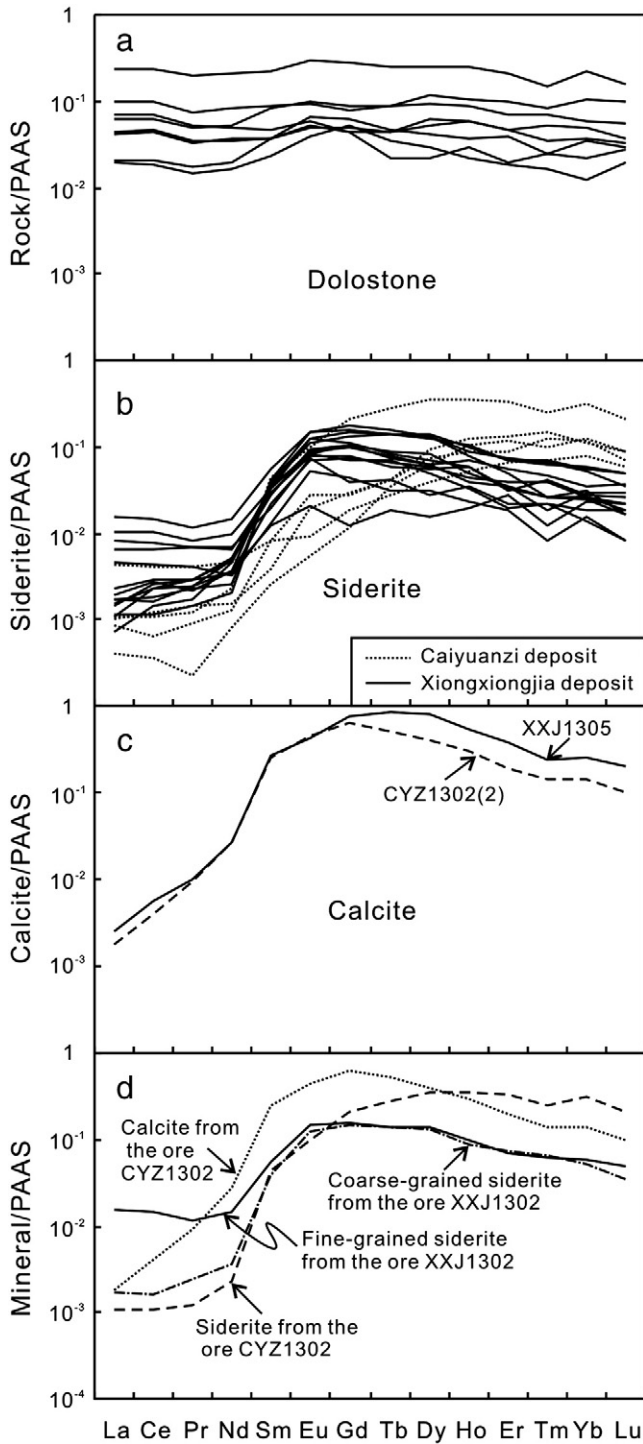
| Sample no.[a] | Sample type[b] | La | Ce | Pr | Nd | Sm | Eu | Gd | Tb | Dy | Ho | Er | Tm | Yb | Lu | $\sum$ REE | $\delta$Eu[c] | $\delta$Ce[c] | (La/Yb)$_N$[d] | (Gd/Yb)$_N$[d] | (La/Sm)$_N$[d] |
|---|---|---|---|---|---|---|---|---|---|---|---|---|---|---|---|---|---|---|---|---|---|
| *Caiyuanzi deposit* | | | | | | | | | | | | | | | | | | | | | |
| CYZ1302A | Sd | 0.041 | 0.088 | 0.011 | 0.072 | 0.247 | 0.106 | 0.991 | 0.221 | 1.55 | 0.360 | 0.950 | 0.127 | 0.870 | 0.106 | 5.74 | 1.00 | 0.95 | 0.00 | 0.68 | 0.02 |
| CYZ1304 | Sd | 0.038 | 0.094 | 0.013 | 0.048 | 0.022 | 0.021 | 0.134 | 0.032 | 0.402 | 0.123 | 0.386 | 0.072 | 0.313 | 0.043 | 1.74 | 1.80 | 0.97 | 0.01 | 0.26 | 0.25 |
| CYZ1307 | Sd | 0.162 | 0.334 | 0.036 | 0.146 | 0.047 | 0.010 | 0.088 | 0.021 | 0.176 | 0.053 | 0.194 | 0.035 | 0.217 | 0.030 | 1.55 | 0.73 | 1.01 | 0.06 | 0.24 | 0.51 |
| CYZ1308 | Sd | 0.032 | 0.051 | 0.008 | 0.042 | 0.045 | 0.031 | 0.131 | 0.032 | 0.324 | 0.088 | 0.261 | 0.061 | 0.321 | 0.034 | 1.46 | 1.88 | 0.73 | 0.01 | 0.24 | 0.10 |
| CYZ1312 | Sd | 0.015 | 0.028 | 0.002 | 0.026 | 0.014 | 0.006 | 0.054 | 0.027 | 0.267 | 0.102 | 0.334 | 0.050 | 0.350 | 0.044 | 1.32 | 1.02 | 1.18 | 0.00 | 0.09 | 0.16 |
| CYZ1302B | Cal | 0.068 | 0.327 | 0.082 | 0.868 | 1.39 | 0.498 | 2.95 | 0.397 | 1.77 | 0.292 | 0.560 | 0.070 | 0.396 | 0.050 | 9.72 | 1.15 | 1.01 | 0.01 | 4.44 | 0.01 |
| *Xiongxiongjia deposit* | | | | | | | | | | | | | | | | | | | | | |
| SMW1302 | Dolostone | 1.70 | 3.64 | 0.304 | 1.14 | 0.208 | 0.054 | 0.229 | 0.033 | 0.279 | 0.058 | 0.138 | 0.026 | 0.135 | 0.018 | 7.97 | 1.15 | 1.16 | 0.93 | 1.01 | 1.21 |
| SMW1303 | Dolostone | 9.18 | 19.2 | 1.77 | 6.67 | 1.26 | 0.320 | 1.30 | 0.188 | 1.08 | 0.248 | 0.620 | 0.076 | 0.619 | 0.078 | 42.60 | 1.17 | 1.10 | 1.09 | 1.25 | 1.08 |
| SMW1304 | Dolostone | 0.733 | 1.47 | 0.129 | 0.515 | 0.133 | 0.042 | 0.238 | 0.026 | 0.129 | 0.022 | 0.052 | 0.008 | 0.035 | 0.010 | 3.55 | 1.10 | 1.10 | 1.54 | 4.05 | 0.81 |
| SMW1305 | Dolostone | 2.60 | 5.44 | 0.473 | 1.56 | 0.265 | 0.064 | 0.206 | 0.034 | 0.232 | 0.057 | 0.138 | 0.017 | 0.104 | 0.016 | 11.20 | 1.28 | 1.13 | 1.84 | 1.18 | 1.45 |
| SMW1306 | Dolostone | 0.782 | 1.67 | 0.154 | 0.621 | 0.212 | 0.057 | 0.201 | 0.017 | 0.097 | 0.029 | 0.058 | 0.012 | 0.060 | 0.014 | 3.99 | 1.29 | 1.11 | 0.96 | 2.00 | 0.54 |
| SMW1307 | Dolostone | 1.58 | 3.40 | 0.291 | 1.17 | 0.202 | 0.071 | 0.285 | 0.035 | 0.183 | 0.036 | 0.110 | 0.012 | 0.098 | 0.015 | 7.50 | 1.38 | 1.15 | 1.19 | 1.73 | 1.16 |
| SMW1308 | Dolostone | 2.30 | 4.99 | 0.433 | 1.69 | 0.477 | 0.106 | 0.411 | 0.068 | 0.415 | 0.090 | 0.199 | 0.034 | 0.167 | 0.027 | 11.41 | 1.12 | 1.15 | 1.02 | 1.47 | 0.71 |
| SMW1309 | Dolostone | 3.78 | 8.10 | 0.662 | 2.62 | 0.490 | 0.105 | 0.363 | 0.069 | 0.506 | 0.106 | 0.289 | 0.041 | 0.297 | 0.048 | 17.48 | 1.16 | 1.18 | 0.94 | 0.73 | 1.14 |
| XXJ1301 | Sd | 0.245 | 0.530 | 0.062 | 0.220 | 0.109 | 0.083 | 0.183 | 0.032 | 0.123 | 0.035 | 0.062 | 0.011 | 0.052 | 0.009 | 1.76 | 2.74 | 0.99 | 0.35 | 2.10 | 0.33 |
| XXJ1302A | Sd | 0.065 | 0.132 | 0.022 | 0.118 | 0.215 | 0.138 | 0.712 | 0.108 | 0.563 | 0.087 | 0.214 | 0.033 | 0.146 | 0.017 | 2.57 | 1.65 | 0.80 | 0.03 | 2.91 | 0.04 |
| XXJ1302B | Sd | 0.573 | 1.17 | 0.100 | 0.459 | 0.303 | 0.163 | 0.750 | 0.106 | 0.620 | 0.101 | 0.203 | 0.031 | 0.160 | 0.025 | 4.77 | 1.59 | 1.13 | 0.26 | 2.79 | 0.28 |
| XXJ1303 | Sd | 0.065 | 0.141 | 0.020 | 0.080 | 0.209 | 0.121 | 0.615 | 0.108 | 0.558 | 0.105 | 0.202 | 0.035 | 0.155 | 0.024 | 2.44 | 1.57 | 0.90 | 0.03 | 2.36 | 0.05 |
| XXJ1306 | Sd | 0.043 | 0.093 | 0.013 | 0.066 | 0.235 | 0.167 | 0.815 | 0.122 | 0.579 | 0.078 | 0.142 | 0.013 | 0.087 | 0.008 | 2.46 | 1.78 | 0.90 | 0.04 | 5.58 | 0.03 |
| XXJ1311 | Sd | 0.056 | 0.206 | 0.025 | 0.156 | 0.168 | 0.092 | 0.334 | 0.053 | 0.212 | 0.033 | 0.057 | 0.011 | 0.038 | 0.004 | 1.45 | 1.81 | 1.27 | 0.11 | 5.24 | 0.05 |
| XXJ1312 | Sd | 0.086 | 0.233 | 0.025 | 0.109 | 0.123 | 0.075 | 0.339 | 0.050 | 0.255 | 0.045 | 0.114 | 0.019 | 0.073 | 0.011 | 1.56 | 1.71 | 1.16 | 0.09 | 2.77 | 0.10 |
| XXJ1313 | Sd | 0.074 | 0.221 | 0.019 | 0.113 | 0.068 | 0.023 | 0.057 | 0.014 | 0.069 | 0.019 | 0.081 | 0.006 | 0.064 | 0.011 | 0.84 | 1.72 | 1.35 | 0.09 | 0.53 | 0.16 |
| XXJ1315 | Sd | 0.170 | 0.336 | 0.037 | 0.102 | 0.071 | 0.056 | 0.202 | 0.024 | 0.134 | 0.023 | 0.053 | 0.004 | 0.043 | 0.004 | 1.26 | 2.18 | 0.97 | 0.29 | 2.80 | 0.35 |
| XXJ1325 | Sd | 0.391 | 0.835 | 0.074 | 0.311 | 0.179 | 0.094 | 0.458 | 0.059 | 0.278 | 0.069 | 0.164 | 0.023 | 0.100 | 0.018 | 3.05 | 1.53 | 1.13 | 0.29 | 2.73 | 0.32 |
| SMW1310 | Sd | 0.027 | 0.114 | 0.015 | 0.143 | 0.182 | 0.133 | 0.533 | 0.065 | 0.306 | 0.057 | 0.094 | 0.013 | 0.070 | 0.008 | 1.76 | 1.99 | 1.30 | 0.03 | 4.54 | 0.02 |
| SMW1313 | Sd | 0.058 | 0.179 | 0.022 | 0.156 | 0.157 | 0.104 | 0.492 | 0.068 | 0.369 | 0.049 | 0.102 | 0.009 | 0.083 | 0.015 | 1.86 | 1.75 | 1.15 | 0.05 | 3.53 | 0.05 |
| SMW1317 | Sd | 0.311 | 0.632 | 0.061 | 0.203 | 0.160 | 0.086 | 0.372 | 0.045 | 0.239 | 0.057 | 0.091 | 0.021 | 0.078 | 0.013 | 2.37 | 1.64 | 1.05 | 0.29 | 2.84 | 0.29 |
| SMW1329 | Sd | 0.041 | 0.178 | 0.025 | 0.161 | 0.190 | 0.089 | 0.504 | 0.056 | 0.266 | 0.040 | 0.103 | 0.013 | 0.072 | 0.009 | 1.75 | 1.34 | 1.28 | 0.04 | 4.17 | 0.03 |
| XXJ1305 | Cal | 0.094 | 0.459 | 0.090 | 0.854 | 1.49 | 0.463 | 3.48 | 0.631 | 3.42 | 0.537 | 1.10 | 0.122 | 0.693 | 0.101 | 13.5 | 0.95 | 1.15 | 0.01 | 2.99 | 0.01 |

[a] CYZ1302A and CYZ1302B denote siderite and calcite separates from the same ore CYZ1302, respectively, whereas XXJ1302A and XXJ1302B represent coarse-grained and fine-grained siderite separates from the same ore XXJ1302, respectively; similarly hereinafter.

[b] Cal, calcite; Sd, siderite.

[c] Eu and Ce anomalies are given as $\delta$Eu $= $Eu$_N$/(Sm$_N$ $\times$ Gd$_N$)$^{0.5}$ and $\delta$Ce $=$ Ce$_N$/(La$_N$ $\times$ Pr$_N$)$^{0.5}$, where values >1 indicate positive anomaly, <1 negative anomaly, and $=$1 no anomaly.

[d] The normalized values of Post-Archean Australian sedimentary rocks (PAAS) are from Nance and Taylor (1976).

**Fig. 8.** PAAS-normalized REE patterns of (a) dolostones, (b) siderite, (c) calcite, and (d) associated mineral pairs. The normalized data of Post-Archean Australian sedimentary rocks (PAAS) are from Nance and Taylor (1976).

**Table 2**
Carbon and oxygen isotopic compositions of carbonates from the Caiyuanzi and Xiongxiongjia deposits.

| Sample no. | Sample type | $\delta^{13}C_{PDB}$ (‰) | $\delta^{18}O_{SMOW}$ (‰) |
|---|---|---|---|
| *Caiyuanzi deposit* | | | |
| CYZ1302A | Siderite | −5.84 | 18.34 |
| CYZ1302B | Calcite | −4.01 | 18.91 |
| CYZ1304 | Siderite | −6.62 | 18.00 |
| CYZ1307 | Siderite | −8.00 | 13.42 |
| *Xiongxiongjia deposit* | | | |
| XXJ1302A | Siderite | −5.71 | 19.22 |
| XXJ1302B | Siderite | −5.09 | 20.07 |
| XXJ1306 | Siderite | −5.40 | 19.70 |
| XXJ1312 | Siderite | −6.31 | 18.36 |
| XXJ1313 | Siderite | −6.82 | 18.19 |
| XXJ1325 | Siderite | −6.14 | 18.68 |
| SMW1313 | Siderite | −5.84 | 18.82 |
| SMW1317 | Siderite | −5.92 | 19.07 |
| SMW1303 | Dolostone | 0.33 | 26.35 |
| SMW1304 | Dolostone | −0.54 | 26.24 |
| SMW1307 | Dolostone | −0.57 | 25.99 |
| SMW1309 | Dolostone | −0.02 | 26.29 |
| XXJ1305 | Calcite | −4.86 | 18.25 |

temperatures and rock/fluid ratios. Siderite was likely to have been derived from the $H_2CO_3$-dominant fluid interacted with marine carbonate with rock/fluid ratios of 0.2 to 0.6 at temperatures of 250 to 150 °C (Fig. 9). Modeling calculations also indicate that calcite possibly derived from the $H_2CO_3$-dominant fluid interacted with marine carbonate with rock/fluid ratios of 0.6 to 0.8 at temperatures of 150 to 100 °C, which is consistent with later formation of calcite than siderite shown by their crosscutting relationships.

### 5.3. Strontium source(s)

Because siderite and calcite contain negligible Rb (<1 ppm) (Table 3), there has been no growth of radiogenic [87]Sr since the crystallization of the carbonates and, thus, the measured Sr isotope ratios represent the Sr isotopic compositions of the parent fluids of the minerals
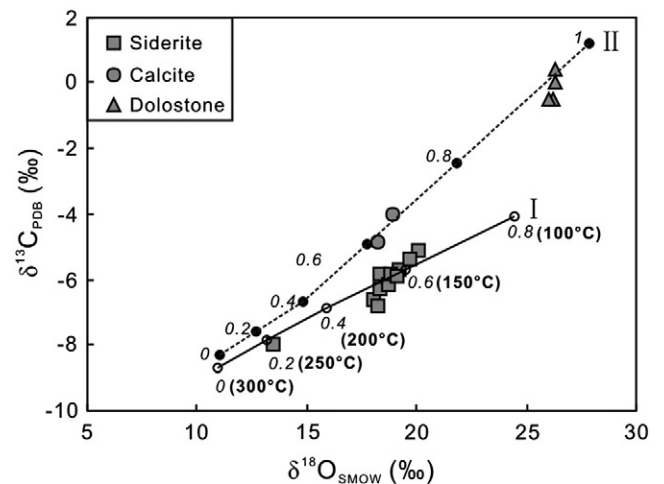


**Fig. 9.** Plot of $\delta^{13}C_{PDB}$ versus $\delta^{18}O_{SMOW}$ values for the host dolostones, siderite, and calcite showing the isotopic results as well as the modeling. The modeling was represented by a fluid–rock interaction in an open system according to Zheng and Hoefs (1993). We assume a marine carbonate with $\delta^{13}C_{PDB}$ = +2‰ and $\delta^{18}O_{SMOW}$ = +28‰ as a protolith, one fluid with −12‰ $\delta^{13}C_{PDB}$ and 6‰ $\delta^{18}O_{SMOW}$ for siderite. The fluid composition for calcite formation was assumed to be −7‰ and 7‰ for C and O isotopes, respectively. In all modeling, we assume that the fluids are $H_2O$-dominant with $(CO_2 + HCO_3^-)/H_2O$ mole ratios of 1:9 and $HCO_3^-$ mole fraction of 0.01. The variations in carbon and oxygen isotopic composition for the protolith during fluid–rock interaction are assumed to be 2.5‰. Line I represents the modeling results of siderite, whereas line II denotes the modeling results of calcite. Different rock/fluid ratios (0, 0.2, 0.4, 0.6, 0.8, 1) and corresponding formation temperatures (300, 250, 200, 150, 100 and 50 °C) are indicated on the lines.

−12‰ $\delta^{13}C_{PDB}$ and 6‰ $\delta^{18}O_{SMOW}$ for siderite. In the calculation of calcite, similar marine carbonate was used as a protolith and fluid composition was assumed to be −7‰ and 7‰ for C and O isotopes, respectively. Using variable fluid–rock ratios, appropriate fractionation factors (Carothers et al., 1988; O'Neil et al., 1969; Sheppard and Schwarcz, 1970), temperatures of 300 to 50 °C, $(CO_2 + HCO_3^-)/H_2O$ mole ratios of 1/9, and $HCO_3^-$ mole fraction of 0.01, final calculated carbonate compositions yield approximating straight line like those illustrated in Fig. 9. Modeling results show that siderite from this study probably formed from different mineralization processes with various

**Table 3**
Strontium isotope data of the dolostones, siderite and calcite from the Caiyuanzi and Xiongxiongjia deposits.

| Sample no. | Sample type | Rb (ppm) | Sr (ppm) | $^{87}Rb/^{86}Sr$ | $(^{87}Sr/^{86}Sr)_m$[a] | $2\sigma$ | $(^{87}Sr/^{86}Sr)_i$[b] |
|---|---|---|---|---|---|---|---|
| Caiyuanzi deposit | | | | | | | |
| CYZ1302A | Siderite | 0.21 | 4.78 | 0.12745 | 0.717789 | 0.000008 | |
| CYZ1302B | Calcite | 0.42 | 181 | 0.00680 | 0.715082 | 0.000009 | |
| CYZ1304 | Siderite | 0.21 | 2.75 | 0.21580 | 0.718086 | 0.000064 | |
| CYZ1307 | Siderite | 0.94 | 5.06 | 0.53706 | 0.717543 | 0.000024 | |
| Xiongxiongjia deposit | | | | | | | |
| SMW1303 | Dolostone | 34.9 | 136 | 0.74466 | 0.712576 | 0.000021 | 0.70844 |
| SMW1304 | Dolostone | 0.90 | 114 | 0.02294 | 0.709231 | 0.000024 | 0.70910 |
| SMW1307 | Dolostone | 3.47 | 125 | 0.08009 | 0.709648 | 0.000013 | 0.70920 |
| SMW1309 | Dolostone | 6.69 | 111 | 0.17388 | 0.709429 | 0.000016 | 0.70846 |
| XXJ1302A | Siderite | 0.42 | 6.59 | 0.18563 | 0.715164 | 0.000014 | |
| XXJ1305 | Calcite | 0.37 | 235 | 0.00459 | 0.715498 | 0.000015 | |
| XXJ1306 | Siderite | 0.23 | 6.53 | 0.10340 | 0.713958 | 0.000065 | |
| XXJ1312 | Siderite | 0.36 | 5.18 | 0.20204 | 0.715249 | 0.000023 | |
| XXJ1313 | Siderite | 0.29 | 2.39 | 0.35068 | 0.717797 | 0.000018 | |
| SMW1313 | Siderite | 0.34 | 10.2 | 0.09664 | 0.714784 | 0.000016 | |

[a] Measured Sr isotopic ratios of samples.
[b] Initial Sr isotope ratios of the dolostones calculated using the decay constant of $1.42 \times 10^{-11}$ a$^{-1}$ and assuming an age of 390 Ma (Middle Devonian). Due to low Rb contents of siderite and calcite, the initial Sr isotope ratios are equal to the measured Sr isotope ratios.

(Frimmel, 1988). The time corrected $(^{87}Sr/^{86}Sr)_i$ values of high-Rb dolostones thus reflect the initial Sr isotopic composition of the reservoir from which the ore-forming fluids have derived their Sr (Frimmel, 1988). The low $(^{87}Sr/^{86}Sr)_i$ values of Devonian dolostones (0.70844 to 0.70920) are close to those of seawater of the same age (0.7078–0.7088) (Burke et al., 1982; Veizer et al., 1999), typical of marine carbonates. The similar Sr isotopic composition of calcite and associated siderite from the same ore indicates a common source. The more radiogenic Sr isotopic composition of siderite and calcite than the host dolostones indicates an additional Sr source for the mineral formation.

The initial Sr isotope ratios of rocks or minerals can be controlled by Rb and Sr contents, formation age, weathering, mineral recrystallization, and fluid metasomatism/mixing (Frimmel, 1988). No obvious correlation between $^{87}Rb/^{86}Sr$ ratio and initial Sr isotope ratio (Fig. 10a)

indicates that Rb and Sr contents may not be the controlling factors for their initial Sr isotopic composition. The linear correlation between initial Sr isotope ratios and the reciprocal of Sr concentrations is consistent with a binary mixing trend (Fig. 10b). This trend can be explained by invoking progressive dilution of Sr-rich mineralizing fluids with a slightly heterogeneous Sr isotope signature by admixture of Sr-poor meteoric waters or reflect a decreasing fluid–rock interaction during the siderite mineralization (Schneider et al., 2003). Low Sr meteoric waters can be excluded because fluid inclusions in siderite were composed of high salinity Na–Cl brines (Liao et al., 1984).

The negative correlation between $(^{87}Sr/^{86}Sr)_i$ and $\delta^{13}C_{PDB}$ and between $(^{87}Sr/^{86}Sr)_i$ and $\delta^{18}O_{SMOW}$ for both the dolostones, siderite and calcite (Fig. 10c and d), also indicates the fluid–rock interaction trend that was proposed for siderite deposits elsewhere (Torres-Ruiz, 2006).
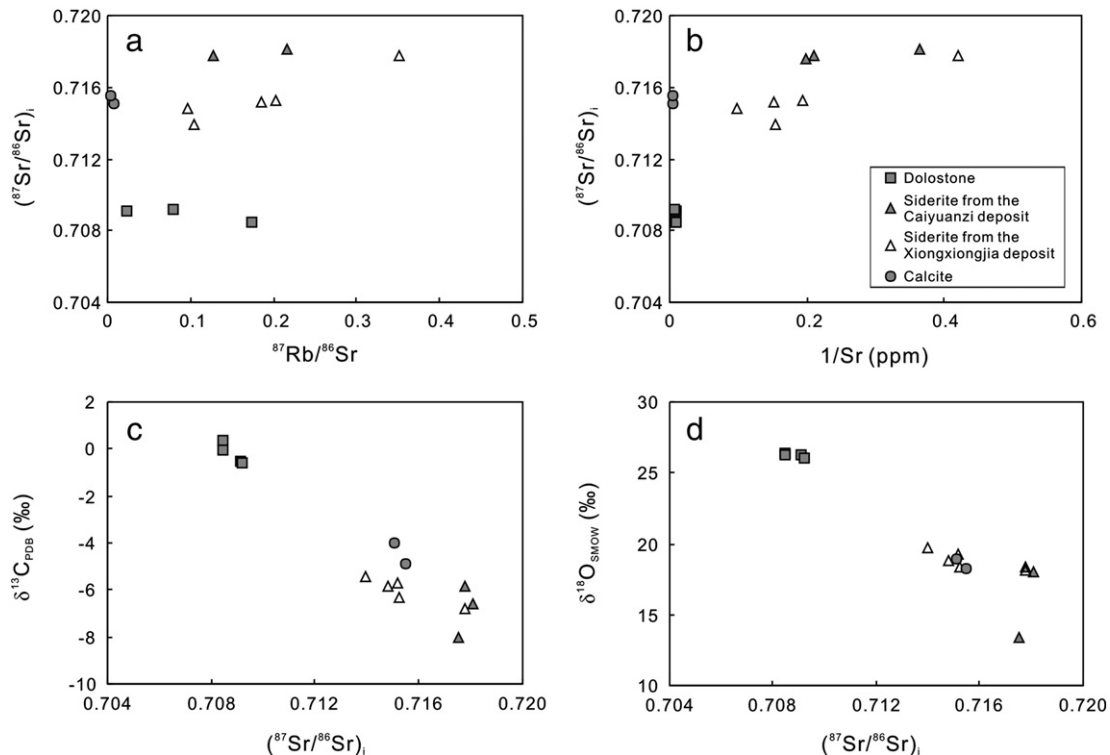


**Fig. 10.** Plots of (a) $(^{87}Sr/^{86}Sr)_i$ versus $^{87}Rb/^{86}Sr$ ratio, (b) $(^{87}Sr/^{86}Sr)_i$ versus 1/Sr, (c) $\delta^{13}C_{PDB}$ versus $(^{87}Sr/^{86}Sr)_i$ and (d) $\delta^{18}O_{SMOW}$ versus $(^{87}Sr/^{86}Sr)_i$ for the host dolostones, siderite and calcite.

**Table 4**
Sulfur isotope data of sulfides from the Caiyuanzi Fe deposit.

| Sample no. | Sample description | Mineral | $\delta^{34}S_{CDT}$ (‰) | Reference |
|---|---|---|---|---|
| CYZ1301 | Banded siderite ore, chalcopyrite is banded | Chalcopyrite | 2.4 | This study |
| CYZ1302 | Banded siderite ore, chalcopyrite is banded | Chalcopyrite | 2.8 | This study |
| CYZ1303 | Massive siderite ore, chalcopyrite is massive aggregate | Chalcopyrite | 11.5 | This study |
| CYZ1304 | Massive siderite ore, chalcopyrite is massive aggregate | Chalcopyrite | 11.0 | This study |
| CYZ1305 | Massive siderite ore, chalcopyrite is massive aggregate | Chalcopyrite | 11.3 | This study |
| CYZ1307 | Massive siderite ore, chalcopyrite is massive aggregate | Chalcopyrite | 11.3 | This study |
| CYZ1308 | Massive siderite ore, chalcopyrite is massive aggregate | Chalcopyrite | 13.6 | This study |
| CYZ1309 | Massive siderite ore, chalcopyrite is massive aggregate | Chalcopyrite | 11.6 | This study |
| CYZ1311 | Massive siderite ore, chalcopyrite is massive aggregate | Chalcopyrite | 10.5 | This study |
| CYZ1312 | Massive siderite ore, chalcopyrite is massive aggregate | Chalcopyrite | 12.1 | This study |
| S901-2 | Massive siderite ore, chalcopyrite is disseminated | Chalcopyrite | 8.4 | Liao et al. (1984) |
| S8954-4 | Massive siderite ore, chalcopyrite is disseminated | Chalcopyrite | 8.3 | Liao et al. (1984) |
| S901-3 | Massive siderite ore, pyrite is massive aggregate | Pyrite | −9.9 | Liao et al. (1984) |
| S8105-473 | Massive siderite ore, pyrite is massive aggregate | Pyrite | −13.8 | Liao et al. (1984) |
| S8105-520 | Massive siderite ore, pyrite is disseminated | Pyrite | 7.8 | Liao et al. (1984) |
| S8105-530 | Massive siderite ore, pyrite is disseminated | Pyrite | 9.1 | Liao et al. (1984) |
| S8105-479 | Fine-grained dolostone, pyrite is banded | Pyrite | −19.9 | Liao et al. (1984) |
| S8105-490 | Dark muddy sandstone, pyrite is disseminated | Pyrite | −16.8 | Liao et al. (1984) |
| S8105-518 | Fine-grained dolostone, pyrite is disseminated | Pyrite | 6.8 | Liao et al. (1984) |
| S8105-460 | Fine-grained dolostone, pyrite is euhedral crystal | Pyrite | 11.6 | Liao et al. (1984) |
| S8105-502 | Oclitic hematite, pyrite is disseminated | Pyrite | 3.4 | Liao et al. (1984) |
| S8105-0 | Clay dolostone, pyrite is disseminated | Pyrite | −11.9 | Liao et al. (1984) |

The dolostones can be metasomatized by later magmatic, metamorphic, or hydrothermal fluids. Magmatic rocks in the study area are dominantly Permian Emeishan flood basalts with minor diabases of unknown



**Fig. 11.** Sulfur isotope histograms of (a) pyrite and chalcopyrite, and (b) sulfides from the wall rocks and the siderite ores.

geochemistry. The basalts have Rb/Sr ratios of 0.007–0.098 similar to those of the siderite and calcite (0.002–0.186) but have age corrected (calculated at 390 Ma) initial Sr isotope ratios (0.70473–0.70624) obviously lower than that of the contemporary siderite and calcite. This indicates that magmatic fluids cannot provide expected radiogenic $^{87}$Sr. Lack of metamorphic events of Sinian to Permian age in the western Guizhou precludes the involvement of metamorphic fluids in the formation of siderite deposits. The Proterozoic Dongchuan and Huili Groups are widely distributed in the western Yangtze Block, and have ($^{87}$Sr/$^{86}$Sr)$_i$ ratios (calculated at 390 Ma) ranging from 0.71543 to 0.72448 (Chen and Ran, 1992; Li and Qin, 1988). The initial Sr isotopic composition of siderite and calcite lies between that of the host dolostones and Proterozoic basement rocks, indicating that the Proterozoic basement rocks are the most likely source for the radiogenic Sr of siderite and calcite.

### 5.4. Sulfur source(s)

Large amounts of sulfides (mainly chalcopyrite and pyrite) along with siderite mineralization occur at the CYZ deposit. Similar sulfur isotopic composition of sulfides from the wall rocks and siderite ores indicate formation of these sulfides by the similar process. The wide range of $\delta^{34}S_{CDT}$ values of sulfides argues against magmatic or magmatic-hydrothermal origins that have sulfur isotopic composition close to zero. The source of sulfur was possibly related to marine sulfates because some sulfides have positive $\delta^{34}S_{CDT}$ values up to +14‰ that are close to those (around +17‰; Claypool et al., 1980) of marine sulfates in the Middle Devonian. The reduction of sulfate can be accomplished either through bacterially mediated processes or abiotic thermochemical processes (Jemmali et al., 2011). Bacterial sulfate reduction can produce sulfate–sulfide fractionations that typically range from ~15 to 60‰ (Goldhaber and Kaplan, 1982), whereas those associated with organic-related thermochemical process range from zero to as much as 10‰ (Kiyosu, 1980; Orr, 1974). Therefore, the negative $\delta^{34}S$ values of pyrite from the Caiyuanzi deposit indicate that part of sulfur probably has derived from bacterial sulfate reduction of marine sulfates, whereas those positive values of pyrite and chalcopyrite may indicate complete reduction of the original sulfates by organic mediated thermochemical processes.

### 5.5. An integrated genetic model for the siderite mineralization

Previous C and O isotopic studies suggested that C and O of siderite were derived from the marine sedimentary process related to
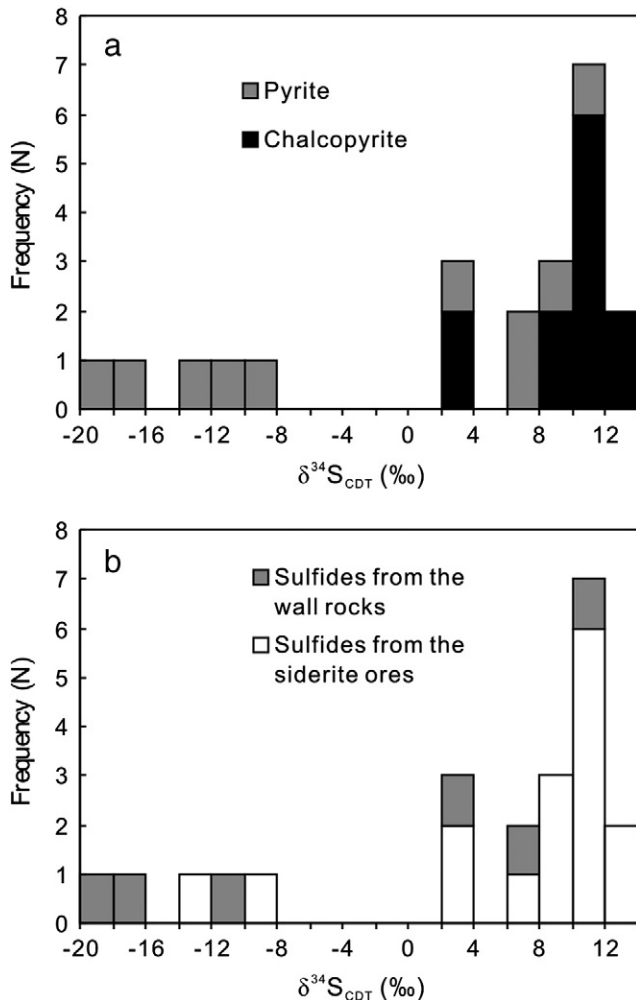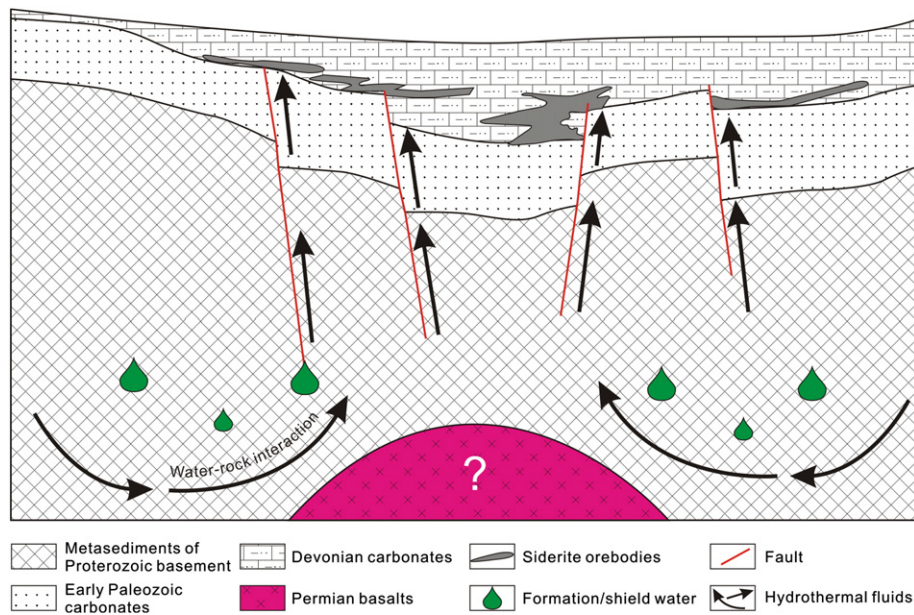
**Fig. 12.** Simple model for the siderite mineralization in western Guizhou. Siderite was formed by the metasomatism of Proterozoic metasediments by deep hydrothermal fluids. The hydrothermal fluids were formed by water–rock interaction between formational or shield brines and Proterozoic basement rocks, possibly heated by Permian basaltic magmatism.

biogeochemistry (Liao et al., 1984). The sulfur of sulfides associated with siderite was considered to be sedimentary origin (Liao et al., 1984). The Caiyuanzi Fe deposit was considered to be a reworked sedimentary deposit (Liao et al., 1984). Combined REE patterns and C, O, Sr and S isotopic compositions from this study supports a metasomatic origin of siderite mineralization at the Caiyuanzi and Xiongxiongjia deposits. Siderite was formed from the replacement of host dolostones by formational or shield brines in Proterozoic basement rocks. Iron was mainly derived from basement leaching rather than continental weathering. An integrated genetic model for siderite mineralization in western Guizhou was illustrated in Fig. 12.

In this model, formation or shield waters in the metasediments of the basement were heated by underlying Permian basaltic magmatism, forming the high temperature (>250 °C), acid, reducing crustal hydrothermal fluids. The hydrothermal fluids ascended along extensional faults and reacted with the organic-rich basement, acquiring abundant Fe and their REE, Sr, C and O isotope features. The hydrothermal fluids vented into the depositional basin and replaced the marine carbonates by fluid–rock interaction. The variation in REE patterns, initial Sr, carbon and oxygen isotopic compositions of siderite and calcite reflect the variable fluid/rock ratios.

## 6. Conclusions

(1) The host dolostones from the Xiongxiongjia (XXJ) deposit in western Guizhou are marine in origin, whereas siderite and calcite from the XXJ and Caiyuanzi (CYZ) deposits were formed by the metasomatic replacement of the dolostones.

(2) Different REE patterns of siderite between the CYZ and XXJ deposits are possibly attributed to variable degrees of fluid–rock interaction. LREE depletion of siderite from the CYZ deposit could be attributed to crystallographic control, whereas LREE depletion and MREE enrichment along with positive Eu anomalies of siderite from the XXJ deposit are typical characteristics of metasomatic siderite.

(3) Modeling indicates that variations in carbon and oxygen isotopic compositions of siderite and calcite were due to metasomatism of the marine carbonates at different fluid/rock ratios under different temperatures.

(4) Strontium in siderite and calcite was most likely derived from the Proterozoic basement rocks. The sulfur of sulfides associated with siderite was derived from marine sulfates in the sedimentary carbonates by bacterial sulfate reduction or organic-related thermochemical reduction.

(5) A genetic model for the siderite mineralization in western Guizhou was proposed. The ore fluids were derived from formation or shield waters in the metasediments of the basement heated by underlying Permian basaltic magmatism. The hot fluids ascended along extensional faults and reacted with the organic-rich basement, acquiring abundant Fe and their REE, Sr, C and O isotope features. Siderite and calcite were formed by replacement of the dolostones by high temperature (>250 °C), acid, reducing crustal hydrothermal fluids at variable fluid/rock ratios.

## References

Baker, J.C., Kassan, J., Hamilton, P., 1996. Early diagenetic siderite as an indicator of depositional environment in the Triassic Rewan Group, southern Bowen Basin, eastern Australia. Sedimentology 43, 77–88.
Bau, M., Möller, P., 1992. Rare earth element fractionation in metamorphogenic hydrothermal calcite, magnesite and siderite. Mineral. Petrol. 45, 231–246.
Burke, W.H., Denison, R.E., Hetherington, E.A., Koepnick, R.B., Nelson, H.F., Otto, J.B., 1982. Variation of seawater $^{87}Sr/^{86}Sr$ throughout Phanerozoic time. Geology 10, 516–519.

Carothers, W.W., Adami, L.H., Rosenbauer, R.J., 1988. Experimental oxygen isotope fractionation between siderite-water and phosphoric acid liberated $CO_2$-siderite. Geochim. Cosmochim. Acta 52, 2445–2450.

Castorina, F., Masi, U., 2008. REE and Nd-isotope evidence for the origin of siderite from the Jebel Awam deposit (Central Morocco). Ore Geol. Rev. 34, 337–342.

Chen, H.S., Ran, C.Y., 1992. Isotope Geochemistry of Copper Deposits in Kangdian Axis. Geological Publishing House, Beijing (in Chinese with English abstract).

Claypool, G.E., Holser, W.T., Kaplan, I.R., Sakai, H., Zak, I., 1980. The age curves of sulfur and oxygen isotopes in marine sulfate and their mutual interpretation. Chem. Geol. 28, 199–260.

Coplen, T.B., 1994. Reporting of stable hydrogen, carbon, and oxygen isotopic abundances. Pure Appl. Chem. 66, 273–276.

Coplen, T.B., Kendall, C., Hopple, J., 1983. Comparison of stable isotope reference samples. Nature 302, 236–238.

Cortecci, G., Frizzo, P., 1993. Origin of siderite deposits from the Lombardy Valleys, northern Italy: a carbon, oxygen and strontium isotope study. Chem. Geol. 105, 293–303.

Ding, T.P., Vaikiers, S., Wan, D.F., Bai, R.M., Zou, X.Q., Li, Y.H., Zhang, Q.L., Bievre, P.D., 2001. The $\delta^{33}S$ and $\delta^{34}S$ values and absolute $^{32}S/^{33}S$ and $^{32}S/^{34}S$ ratios of IAEA and Chinese sulfur isotope reference materials. Bull. China Soc. Mineral. Petrol. Geochem. 20, 425–427 (in Chinese with English abstract).

Elderfield, H., Greaves, M.J., 1982. The rare earth elements in seawater. Nature 296, 214–219.

Frimmel, H., 1988. Strontium isotopic evidence for the origin of siderite, ankerite and magnesite mineralizations in the Eastern Alps. Mineral. Deposita 23, 268–275.

Gao, S., Yang, J., Zhou, L., Li, M., Hu, Z., Guo, J., Yuan, H., Gong, H., Xiao, G., Wei, J., 2011. Age and growth of the Archean Kongling terrain, South China, with emphasis on 3.3 Ga granitoid gneisses. Am. J. Sci. 311, 153–182.

Goldhaber, M.B., Kaplan, I.R., 1982. Controls and consequences of sulfate reduction rates in recent marine sediments. Acid Sulfate Weathering 119, 19–36.

Hecht, L., Freiberger, R., Gilg, H.A., Grundmann, G., Kostitsyn, Y.A., 1999. Rare earth element and isotope (C, O, Sr) characteristics of hydrothermal carbonates: genetic implications for dolomite-hosted talc mineralization at Göpfersgrün (Fichtelgebirge, Germany). Chem. Geol. 155, 115–130.

Hu, X., Wang, Y.L., Schmitt, R.A., 1988. Geochemistry of sediments on the Rio Grande Rise and the redox evolution of the South Atlantic Ocean. Geochim. Cosmochim. Acta 52, 201–207.

Huang, X.W., Zhao, X.F., Qi, L., Zhou, M.F., 2013. Re–Os and S isotopic constraints on the origins of two mineralization events at the Tangdan sedimentary rock-hosted stratiform Cu deposit, SW China. Chem. Geol. 347, 9–19.

Irwin, H., Curtis, C., Coleman, M., 1977. Isotopic evidence for source of diagenetic carbonates formed during burial of organic-rich sediments. Nature 269, 209–213.

Jemmali, N., Souissi, F., Villa, I.M., Vennemann, T.W., 2011. Ore genesis of Pb–Zn deposits in the Nappe zone of Northern Tunisia: constraints from Pb–S–C–O isotopic systems. Ore Geol. Rev. 40, 41–53.

Kiyosu, Y., 1980. Chemical reduction and sulfur-isotope effects of sulfate by organic matter under hydrothermal conditions. Chem. Geol. 30, 47–56.

Li, F.H., Qin, J.M., 1988. Presinian System in Kangdian Area. Chongqing Press, Chongqing (in Chinese with English abstract).

Li, H.Z., Wu, D.S., Han, Z.J., Wang, Y.G., Wang, P.F., Hu, K.C., Liu, X.F., 1996. The Discovery History of Mineral Deposits of China—Guizhou Volume. Geological Publishing House, Beijing (in Chinese with English abstract).

Liao, S.F., Liang, T.R., Zeng, M.G., Meng, X.L., Yang, J.Q., 1980. Metallogenic patterns and principles of modified Tiekuangshan sedimentary siderite deposit. Geol. Rev. 26, 16–25 (in Chinese).

Liao, S.F., Liang, T.R., Meng, X.L., Zeng, M.G., Chen, S.J., Zeng, L.S., Yan, C.X., Liu, X.F., 1984. A Study on the Reworked Sedimentary Siderite Deposits in West Guizhou. Geological Publishing House, Beijing, China (in Chinese with English abstract).

Lin, L.Q., Chen, Z.Y., Wan, H.Q., Xu, A.P., Ling, Y.C., 1986. The characteristics of hydrogen, oxygen and carbon isotopes and their geological significance of Caiyuanzi siderite deposit. Geol. Guizhou 240–247 (in Chinese with English abstract).

Lüders, V., Möller, P., Dulski, P., 1993. REE fractionation in carbonates and fluorite. In: Möller, P., Lüders, V. (Eds.), Formation of Hydrothermal Vein Deposits. Gebrüder Bornträeger, Berlin-Stuttgart, pp. 133–150.

Michard, A., 1989. Rare earth element systematics in hydrothermal fluids. Geochim. Cosmochim. Acta 53, 745–750.

Morgan, J.W., Wandless, G.A., 1980. Rare earth element distribution in some hydrothermal minerals: evidence for crystallographic control. Geochim. Cosmochim. Acta 44, 973–980.

Nance, W.B., Taylor, S., 1976. Rare earth element patterns and crustal evolution—I Australian post-Archean sedimentary rocks. Geochim. Cosmochim. Acta 40, 1539–1551.

O'Neil, J.R., Clayton, R.N., Mayeda, T.K., 1969. Oxygen isotope fractionation in divalent metal carbonates. J. Chem. Phys. 51, 5547.

Orr, W.L., 1974. Changes in sulfur content and isotopic ratios of sulfur during petroleum maturation; study of big horn basin Paleozoic oils. AAPG Bull. 58, 2295–2318.

Palinkaš, S.S., Spangenberg, J.E., Palinkaš, L.A., 2009. Organic and inorganic geochemistry of Ljubija siderite deposits, NW Bosnia and Herzegovina. Mineral. Deposita 44, 893–913.

Qi, L., Grégoire, D.C., 2000. Determination of trace elements in twenty-six Chinese geochemistry reference materials by inductively coupled plasma-mass spectrometry. Geostand. Newslett. 24, 51–63.

Qi, L., Zhou, M.-F., 2008. Platinum-group elemental and Sr–Nd–Os isotopic geochemistry of Permian Emeishan flood basalts in Guizhou Province, SW China. Chem. Geol. 248, 83–103.

Qiu, Y.M., Gao, S., McNaughton, N.J., Groves, D.I., Ling, W., 2000. First evidence of >3.2 Ga continental crust in the Yangtze craton of south China and its implications for Archean crustal evolution and Phanerozoic tectonics. Geology 28, 11–14.

Rangarajan, R., Ghosh, P., 2011. Role of water contamination within the GC column of a GasBench II peripheral on the reproducibility of $^{18}O/^{16}O$ ratios in water samples. Isot. Environ. Health Stud. 47, 498–511.

Savard, M.M., Sangster, D.F., Buntt, M.D., 1998. Isotope geochemistry of sideritized host rocks, Walton Ba deposit, Kennetcook Sub-basin, Nova Scotia, Canada. Econ. Geol. 93, 834–844.

Schneider, J., Haack, U., Stedingk, K., 2003. A Sr isotope study on fluorite and siderite from post-orogenic mineral veins in the eastern Harz Mountains, Germany. Mineral. Deposita 38, 984–991.

Sheppard, S.M., 1986. Characterization and isotopic variations in natural waters. Rev. Mineral. Geochem. 16, 165–183.

Sheppard, S.M., Schwarcz, H.P., 1970. Fractionation of carbon and oxygen isotopes and magnesium between coexisting metamorphic calcite and dolomite. Contrib. Mineral. Petrol. 26, 161–198.

Sun, W.H., Zhou, M.F., Gao, J.F., Yang, Y.H., Zhao, X.F., Zhao, J.H., 2009. Detrital zircon U–Pb geochronological and Lu–Hf isotopic constraints on the Precambrian magmatic and crustal evolution of the western Yangtze Block, SW China. Precambrian Res. 172, 99–126.

Timofeyeva, Z., Kuznetsova, L., Dontsova, Y.I., 1976. Oxygen isotopes and siderite formation. Geochem. Int. 13, 101–112.

Torres-Ruiz, J., 2006. Geochemical constraints on the genesis of the Marquesado iron ore deposits, Betic Cordillera, Spain: REE, C, O, and Sr isotope data. Econ. Geol. 101, 667–677.

Veizer, J., Hoefs, J., 1976. The nature of $O^{18}/O^{16}$ and $C^{13}/C^{12}$ secular trends in sedimentary carbonate rocks. Geochim. Cosmochim. Acta 40, 1387–1395.

Veizer, J., Ala, D., Azmy, K., Bruckschen, P., Buhl, D., Bruhn, F., Carden, G.A., Diener, A., Ebneth, S., Godderis, Y., 1999. $^{87}Sr/^{86}Sr$, $\delta^{13}C$ and $\delta^{18}O$ evolution of Phanerozoic seawater. Chem. Geol. 161, 59–88.

Yan, D.-P., Zhou, M.-F., Song, H.-L., Wang, X.-W., Malpas, J., 2003. Origin and tectonic significance of a Mesozoic multi-layer over-thrust system within the Yangtze Block (South China). Tectonophysics 361, 239–254.

Zhao, X.F., 2010. Paleoproterozoic Crustal Evolution and Fe–Cu Metallogeny of the Western Yangtze Block, SW China. The University of Hongkong, Hongkong.

Zhao, J.H., Zhou, M.F., Yan, D.P., Zheng, J.P., Li, J.W., 2011. Reappraisal of the ages of Neoproterozoic strata in South China: no connection with the Grenvillian orogeny. Geology 39, 299–302.

Zheng, Y.F., Chen, J.F., 2000. Stable Isotope Geochemistry. Science Press, Beijing (in Chinese).

Zheng, Y.-F., Hoefs, J., 1993. Carbon and oxygen isotopic covariations in hydrothermal calcites: theoretical modeling on mixing processes and application to Pb–Zn deposits in the Harz Mountains, Germany. Mineral. Deposita 28, 79–89.

Zhou, M.F., Yan, D.P., Kennedy, A.K., Li, Y., Ding, J., 2002. SHRIMP U–Pb zircon geochronological and geochemical evidence for Neoproterozoic arc-magmatism along the western margin of the Yangtze Block, South China. Earth Planet. Sci. Lett. 196, 51–67.

Zhou, J.C., Wang, X.L., Qiu, J.S., 2009. Geochronology of Neoproterozoic mafic rocks and sandstones from northeastern Guizhou South China: coeval arc magmatism and sedimentation. Precambrian Res. 170, 27–42.